



Research Paper

No more blind dates with calcite: Fluid-flow vs. fault-slip along the Očkov thrust, Prague Basin

Nick M.W. Roberts ^{a,*}, Jiří Žák ^b, František Vacek ^{b,c}, Jiří Sláma ^d

^a Geochronology and Tracers Facility, British Geological Survey, Environmental Science Centre, Nottingham NG12 5GG, UK

^b Institute of Geology and Paleontology, Faculty of Science, Charles University, Albertov 6, Prague 12843, Czech Republic

^c Department of Mineralogy and Petrology, National Museum, Václavské náměstí 68, Prague 11579, Czech Republic

^d Institute of Geology, Czech Academy of Sciences, v.v.i., Rozvojová 269, Prague 16500, Czech Republic

ARTICLE INFO

Article history:

Received 28 October 2020

Received in revised form 31 December 2020

Accepted 4 January 2021

Available online 13 January 2021

Editor: M. Santosh

Keywords:

U-Pb geochronology

Calcite

Fault dating

Fluid-flow

Prague Basin

LA-ICP-MS

ABSTRACT

Dating of fracture-filling calcite with U-Pb geochronology is becoming a rapidly adopted technique for determining the absolute timing of brittle deformation in the upper crust. Slickenfibres calcite is a desirable target, as it precipitates between individual fault slip displacement events, and provides additional kinematic information. Here we present a case study of slickenfibres formed on the Očkov thrust in the Lower Palaeozoic Prague Basin, Bohemian Massif, utilising a combination of petrographic and in situ methods. We demonstrate that slickenfibre external textures can be preserved, whilst internally primary textures are removed by fluid infiltration and recrystallization, leading to variable U and Pb mobilisation. One slickenfibre yielded a date of ca. 250 Ma, which we interpret as recording fault slip along the Očkov thrust. Another cross-cutting slickenfibre yielded more scattered U-Pb data, with an imprecise apparent age around ca. 95 Ma. This slickenfibre is recrystallised, destroying the primary textures, and exhibits element mobility. The meaning of this younger apparent age is therefore questionable; whereas it likely reflects Cretaceous U and Pb mobility assisted by fluid-flow along the fault plane, it may not reflect a period of fault slip. Our results demonstrate that slickenfibre-based U-Pb dates do not unequivocally relate to fault motion, and that petrographic and elemental analyses are important requirements for interpreting calcite U-Pb data.

© 2021 Elsevier B.V. This is an open access article under the CC BY-NC-ND license (<http://creativecommons.org/licenses/by-nc-nd/4.0/>).

1. Introduction

Dating of brittle deformation has lacked robust techniques that are applicable to a wide-range of fracture, folding and faulting styles. The development of in situ U-Pb geochronology of carbonates (Li et al., 2014; Coogan et al., 2016; Roberts et al., 2020a) has opened the doors to a new method that is widely applicable, since carbonate mineralisation is common to many settings of brittle deformation, and uses instrumentation that is widespread in many isotope geochemical facilities globally – Laser Ablation Inductively Coupled Mass Spectrometry (LA-ICP-MS). Roberts and Walker (2016) and Ring and Gerdes (2016) were the first to demonstrate the technique to dating of brittle faulting episodes, and the technique has been rapidly adopted (e.g. Goodfellow et al., 2017; Nuriel et al. 2017, 2019; Hansman et al., 2018; Parrish et al., 2018; Holdsworth et al., 2019; Smeraglia et al., 2019; Mottram et al., 2020; Oren et al., 2020; Roberts et al., 2020b; Weinberger et al., 2020; Hoareau et al., 2021). Roberts and Walker (2016) used LA-ICP-MS U-Pb to date calcite vein-fills located within major fault structures cross-cutting the Palaeogene Faroe Islands plateau basalt sequence. These authors used

crack-seal-slip calcite textures, generally comprising veins with syntaxial growth, to indicate that the obtained dates were capturing precipitation of calcite between individual slip events along the fault structures. Other approaches have been to use calcite slickenfibres that have precipitated along fault planes (Ring and Gerdes 2016; Nuriel et al. 2017, 2019; Miranda et al., 2020; Mottram et al., 2020), calcite cements within fault implosion breccias (Roberts and Walker 2016; Simpson et al., 2021), or kinematically constrained vein sets associated with fracturing and/or folding (Beaudoin et al., 2018, 2020; Parrish et al., 2018; Hoareau et al., 2021; Roberts et al., 2020b).

There is a key premise to dating deformation with calcite mineralisation: calcite precipitation must have occurred shortly after or between fault slip events. Many authors have used the term “directly dating”, but in a strict sense this is a misnomer since fault slip is normally composed of discrete slip events, even with slow creep of faults, and precipitation of calcite occurs after each fault slip or fracture-opening event. If the dated calcite vein is cut by later fault slip planes, then it can be presumed to capture an episode of faulting within the total timeframe of fault slip. At present, there are few studies documenting the absolute growth history of calcite vein in-fills. Williams et al. (2017) presented multiple U-Th dates from crack-seal calcite veins, demonstrating that where multiple calcite generations were sampled from the same vein, these were formed

* Corresponding author.

E-mail address: nirob@bgs.ac.uk (N.M.W. Roberts).

within 10,000s years of each other, i.e. well within the uncertainty of any U-Pb date. Williams et al. (2019) furthered this insight with dates along the length of individual calcite growth phases within crack-seal veins, demonstrating growth rates of between 0.05 and 0.80 km/ka.

Another key premise to the linking of dates with deformation is the assumption that the calcite mineralisation, and explicitly the U-Pb isotopic system, has not been altered or reset. This may occur by fluid influx and alteration, or by complete recrystallization of the primary calcite. Such events have not received detailed documentation in the literature in the context of their geochronology. Studies assessing the viability of carbonate geochronology have focused on U-Th dating of speleothems (e.g. Scholz et al., 2014; Bajo et al., 2016), or were conducted with bulk dissolution methods prior to the advent of high spatial resolution methods such as LA-ICP-MS (e.g. DeWolf and Halliday 1991; Smith et al., 1991). There are various means to address the primary nature of calcite mineralisation, but in many cases the information is equivocal. The common method is to use petrographic imaging, and for carbonates this typically comprises cathodoluminescence imaging (CL; see Machel, 1985, 2000). CL is dominated by chemical zonation, and offers high spatial resolution. Other electron and optical microscopic techniques include Back Scattered Electron, Charge Contrast Imaging and reflected light (see Roberts et al., 2020a). Each of these techniques pick out a combination of structural and chemical information which can be used to evaluate the nature of the calcite in question, and whether it represents primary precipitate, or is partially to completely altered/reprecipitated. Another approach is to combine petrographic imaging with elemental mapping. This can be achieved through Secondary Electron Microscope, Electron Microprobe or LA-ICP-MS, with the latter more suitable for trace elements due to its lower detection limits. Roberts and Walker (2016) used this approach to characterise the U and Pb distribution in their dated calcite veins, with the simple assumption that correlation between U and other major and trace elements implies a lack of U mobility, and that the dates can be deemed to be robust. This method is only qualitative, in a similar manner to using spider-diagrams to assess elemental mobility in whole-rock geochemistry, but there is a lack of alternative methods for unequivocally characterising the mobility and alteration of calcite chemistry.

Although calcite U-Pb geochronology is now being widely applied, many studies do not offer comprehensive documentation of the dated material. As such, primary calcite is merely assumed, and the readers have to take it upon faith that the dates represent the deformation or fluid-flow event that the authors present. Here we present petrographic imaging, and elemental and isotopic data from a case study of calcite slickenfibres taken from the Očkov thrust in the Lower Paleozoic Prague Basin, Bohemian Massif (Fig. 1a, b). The data reveal that although the gross macrostructure of calcite is preserved, the internal textures imply partial localised to complete recrystallization. The geochronological question then becomes what do the U-Pb dates for the variously disturbed calcite domains mean? This case study is, therefore, a cautionary tale against the blind use of calcite mineralisation to date deformation.

2. Geological setting

The Prague Basin is a prominent structure in the central Bohemian Massif, Variscan belt (Fig. 1a, b), which formed as a narrow, fault-bounded graben on the extensive peri-Gondwana shelf during lithospheric extension related to opening of the Rheic Ocean (e.g. Chlupáč et al., 1998; Nance et al., 2010; Žák et al., 2013 and references therein). The basin is filled with a continuous volcano-sedimentary marine succession ranging from the earliest Ordovician (Tremadocian) to Middle Devonian (Givetian; Fig. 1b). During the Variscan orogeny, the northwesterly Saxothuringian Ocean and the adjacent continental margin were progressively subducted beneath the overriding plate (Teplá-Barrandian unit) with the Prague Basin on top (from >380 Ma to 340 Ma; e.g. Schulmann et al. 2009, 2014). This resulted in basin inversion, uplift, and folding and faulting due to NW-SE to WNW-ESE horizontal

shortening (e.g. Havlíček 1963, 1981; Chlupáč et al. 1998; Zulauf 2001; Melichar 2004; Röhlich 2007; Hajná et al. 2012; Vacek and Žák 2019). Fluid inclusion studies estimate the maximum palaeodepth of about 2–3 km (within the oil window) for the uppermost (Givetian) strata in the basin (e.g. Suchý et al., 1996; Halavínová et al., 2008; Slobodník et al., 2012). The style and intensity of the Variscan deformation varies along strike in two contrasting segments of the basin (Röhlich 2007). The northeastern segment forms a 36 km long and 16 km wide NE-SW-trending syncline (Fig. 1b). The southwestern segment comprises a mosaic of fault-bounded blocks, with bedding attitude varying from one block to another, from commonly flat to rarely steep.

The tectonic evolution of the Prague syncline was described in detail by Vacek and Žák (2019). The overlap successions suggest that the syncline underwent pre-314 Ma uplift and denudation, constrained by the base of the overlying late Carboniferous intra-continental coal basins (e.g. Opluštil and Cleal 2007; Opluštil et al., 2016), and was partly below sea level during the Late Cretaceous (Cenomanian) marine transgression. The interpretation of existing apatite fission-track data in the Prague syncline are debated, but potentially indicate a complex post-Variscan history of burial and denudation/uplift (e.g. Glasmacher et al., 2002; Suchý et al., 2002; Filip and Suchý 2004). Multiple intra-plate tectonic events have been recognized elsewhere in the Bohemian Massif from the late Carboniferous to Quaternary (e.g. Malkovský 1987; Ventura and Lisker 2003; Danišik et al. 2010, 2012; Coubal et al., 2015, and references therein), and are thus also likely to affect the Prague syncline by brittle fracturing and reactivation of inherited structures.

The Prague syncline is cross-cut by a complex system of faults of various dimensions, amounts of displacement, ages (from syn-depositional to post-Cretaceous), and kinematics. The Očkov fault, with a total displacement of about 2.5 km (Röhlich 2007), belongs to a population of reverse and thrust faults that are documented mostly within the Silurian-Devonian core of the syncline (Fig. 1b, c). These major reverse and thrust faults extend for several kilometres or even tens of kilometres in length, their traces are roughly parallel to lithological contacts, and they are doubly vergent with opposite dips and hangingwall transport directions in each limb of the Prague syncline. At outcrop, the faults are expressed either as single, knife-sharp fault planes (Fig. 2) or comprise up to several metres thick zones of anastomosing smaller faults with associated fault breccia, intensely developed pressure-solution cleavage, and metre-scale folds. In addition, a number of minor, small-scale reverse and thrust faults are documented within the Silurian-Devonian succession in association with duplexes and folds.

3. Samples

The Očkov fault is one of the major reverse/thrust faults that cut the Prague syncline and thrusts a late Silurian succession over an Early Devonian footwall (Fig. 1c). The fault was mapped previously in great detail (e.g. Chlupáč 1989; Adamovič 2002) and is superbly exposed in several disused quarries along its length (Fig. 2). At map-scale, the fault strikes WSW in the west and then bends into a dominant WNW strike in its central portion and in the east (Fig. 1c). The fault plane may be locally curved and irregular in detail, but generally dips to N and NNE at a moderate to steep angle.

The samples were taken in a disused quarry 'Čisářský lom' (approximately 360 m SSW of Koněprusy; WGS84 coordinates: 49.9177167°N, 14.0640814°E; Fig. 1c). At this locality, the Očkov fault strikes to the W (ca. 260°–280°) and dips to the N at a moderate to steep angle (ca. 50°–80°). The fault places the upper Silurian thinly bedded limestones and calcareous shales (Požáry Fm., Přídolí) in the hanging wall over coarse-grained, non-bedded Lower Devonian biotrititic limestones (Koněprusy Limestone of the Praha Fm., Pragian) in the footwall. The hanging wall limestone-shale succession has been folded into tight, upright, E-W-trending chevron folds. The fold axes are parallel to the fault

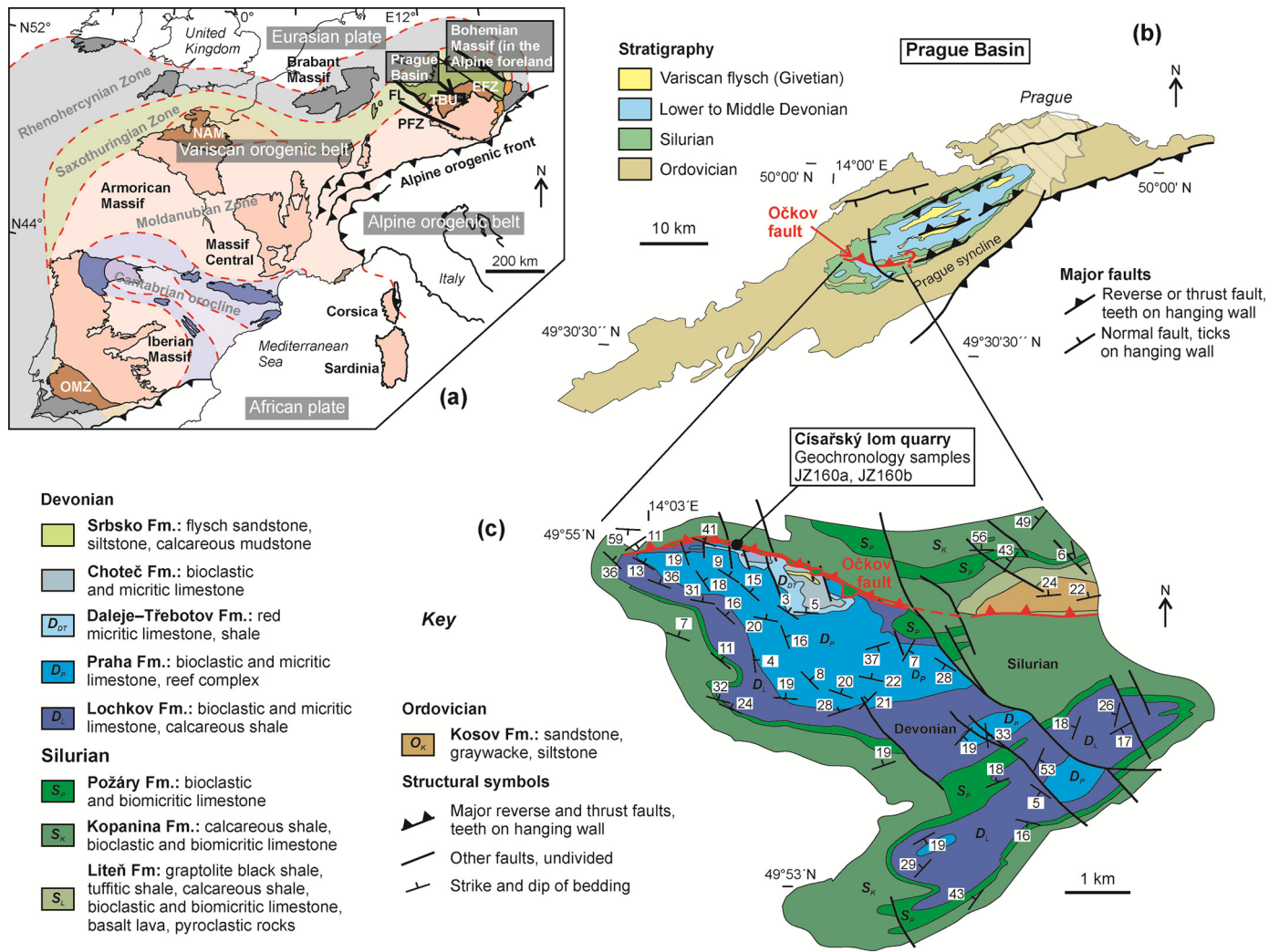


Fig. 1. (a) Simplified geological map showing principal lithotectonic zones and basement outcrop areas of the Variscan orogenic belt in Europe. The Bohemian Massif is the northeasternmost inlier of the orogen and now occupies an intra-plate position in the Alpine foreland. Remnants of the Variscan upper crust, including the Teplá–Barrandian unit (TBU) with the Prague Basin, are shown in brown colour (NAM – North Armorican Massif, OMZ – Ossa Morena Zone). Compiled from Winchester (2002) and Martínez Catalán (2012). Fault zones relevant to this study: EFZ – Elbe fault zone, FL – Franconian lineament, PFZ – Pfahl fault zone. (b) Greatly simplified lithotectonic scheme of the Prague Basin to show location of the Očkov fault. (c) Simplified geological map of the southwestern part of the Prague syncline showing the Očkov fault and vicinity. Simplified from Vacek and Žák (2019). (For interpretation of the references to color in this figure legend, the reader is referred to the web version of this article.)

plane but their limbs are cut off by the fault. This observation suggests that they formed during the same N-S compression, but that the fault movements continued after flexural-slip folding.

Four different generations of calcite slickenfibres were recognized on the fault plane at this outcrop (Fig. 2b). The dated samples were taken as small chips, several centimetres across, from the two relatively oldest generations of these slickenfibres (Fig. 2c and d). The earliest slickenfibres are oriented down-dip (sample 160a). The other dated sample, 160b, is dip-oblique and successively overgrows the earlier generation. The multiple generations of slickenfibres at this outcrop indicate at least three distinct, superposed phases of early dip-slip and oblique-slip thrusting along the Očkov fault. Chips of each calcite sample were mounted in epoxy and cut orthogonal to the slickenfibre surface.

4. Methods

4.1. CL imaging

CL imaging was undertaken at the British Geological Survey (Nottingham, UK) using a Technosyn 8200 MkII cold-cathode luminescence

stage attached to a Nikon optical microscope with long working distance lenses, and equipped with a Zeiss AxioCam MRC5 digital camera. The vacuum and electron beam voltage and current were adjusted as required to generate optimum luminescence.

4.2. Trace elements

LA-ICP-MS trace element data were collected at the Geochronology and Tracers Facility, British Geological Survey (Nottingham, UK), using a New Wave Research (ESL) 193UC excimer laser ablation system fitted with a TV2 cell coupled to a Nu Instruments Atom single collector ICP-MS. Elemental maps of specific calcite chips were generated by rastering a 100 µm × 100 µm across a rectangular region at a rate of 50 µm per second, and normalising to NIST614 glass (values of Jochum et al., 2011), using ⁴⁴Ca as an internal standard, and assuming stoichiometric Ca contents in calcite. Iolite software was used for map creation (Paton et al., 2011). Trace element ‘spot’ data were obtained using the same analytical conditions and normalisation, but with 100 µm diameter static 30 s spots. Full datasets and analytical conditions are provided in the Electronic Supplementary Material.

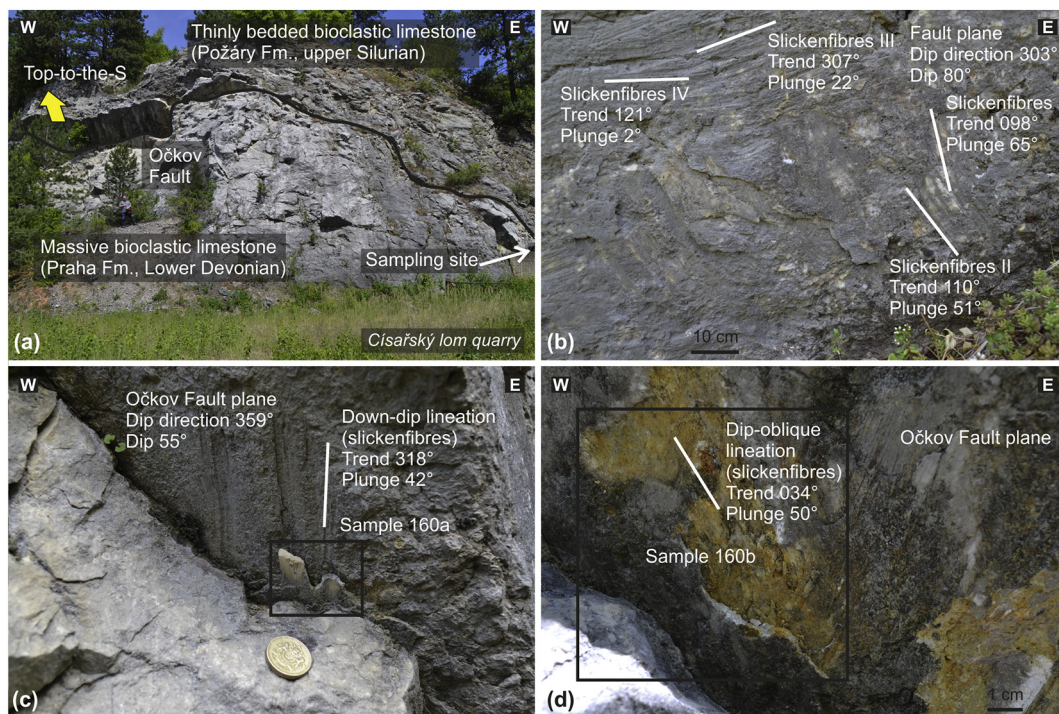


Fig. 2. Field photographs to show the Očkov Fault and associated small-scale features. (a) Exposure of the Očkov Fault in the Cisařský lom quarry, WGS84 coordinates: 49.9176797°N, 14.0638789°E. (b) Fault plane adjacent to the Očkov Fault bearing four different generations of superposed calcite slickenfibres (marked as I–IV) that indicate polyphase fault reactivation. WGS84 coordinates: 49.9175553°N, 14.0646808°E. (c) Close-up view on sample 160a (before sampling) which represents the oldest dip-slip movements along the Očkov Fault. WGS84 coordinates: 49.9177167°N, 14.0640814°E. (d) Close-up view on the Očkov Fault plane with younger dip-oblique slickenfibres sampled for U–Pb geochronology (sample 160b). WGS84 coordinates same as for (d).

4.3. U–Pb geochronology

U–Pb geochronology was conducted using the same instrumentation as the trace element analysis. The method follows that described in Roberts et al. (2017), and full data and analytical conditions are provided in the Electronic Supplementary Material. In brief, screening was conducted using traverses of 100 μm spots across calcite chips, with standard-sample bracketing using WC-1 calcite reference material (Roberts et al., 2017). Domains of interest (i.e. those with high U/Pb ratios) were revisited for further detailed spot analyses. During the latter analytical sessions, another material with a known age determined by isotope dilution (Duff Brown Tank, 64.04 ± 0.67 Ma; Hill et al., 2016) was measured to check on accuracy, and gave a pooled age of 64.36 ± 0.88 Ma (2s).

5. Results

5.1. Imaging

5.1.1. Sample 160a

Chips of sample 160a (Fig. 3) are variably cloudy to milky, with three chips exhibiting more transparent sparry calcite. Discolouration at the surface of the larger chips indicated alteration due to weathering, and this has pervaded the slickenfibres in a few places, presumably along veinlets. We have divided the chips into three textural varieties, sparry, milky and zebra-striped, and characterised four chips exhibiting these textures in detail. Two chips (5 and 6) are comprised of sparry calcite. These both exhibit weak planar zoning patterns in CL, which we interpret as primary growth zoning. Both CL and optical imagery show some fractures and minor veining. A small pyramid-shaped region of chip 3 also shows a sparry texture, and similar growth zoning in CL to chips 5 and 6. This domain forms the upper surface of the slickenfibres. Chip 3 reveals two other domains, a region of ‘zebra-striped’ calcite, and a region of milky calcite; these are separated by a wavy margin

that is visible optically, and shows up bright in CL. The zebra-striped region reveals zoning that is not perfectly planar, but reveals disturbances to the continuity of the striping. It is not clear whether this represents structural deformation of the calcite after the calcite precipitation, or changes in growth direction during precipitation due to continued slip along the fault. The fourth chip is entirely composed of milky calcite. The milky domains are interpreted as resulting from microscopic inclusions (although we could not verify their presence), and the microcrystalline rather than coarse-crystalline texture. The CL signature of the milky regions is faintly mottled, but otherwise rather featureless.

5.1.2. Sample 160b

Chips of sample 160b (Fig. 3) are variably milky, with two chips comprising less milky and more transparent domains, and three chips being more dominantly milky and opaque. Two chips (1 and 4) were examined in more detail, covering both opaque and transparent domains. The opaque chip (4) has discoloured regions in various areas, including a veinlet cutting all the way across the chip.

The remaining regions are mottled with no clear primary structure. The second chip (1) is mottled, varying between more and less opaque. A few veinlets are visible optically cross the chip; only a couple of these show up as brighter veins in CL. The CL response of the opaque regions are mottled and lack primary structures. In chip 4, only one very small region exhibits some planar zoning which we interpret as a remnant of primary growth zoning. The CL of chip 1 is more variable, and exhibits more evidence of primary growth zoning.

5.2. Trace elements

5.2.1. Sample 160a

Trace element maps are shown of one chip in Fig. 4a. All elements reveal the same shape to their enrichment/depletion, which is broadly

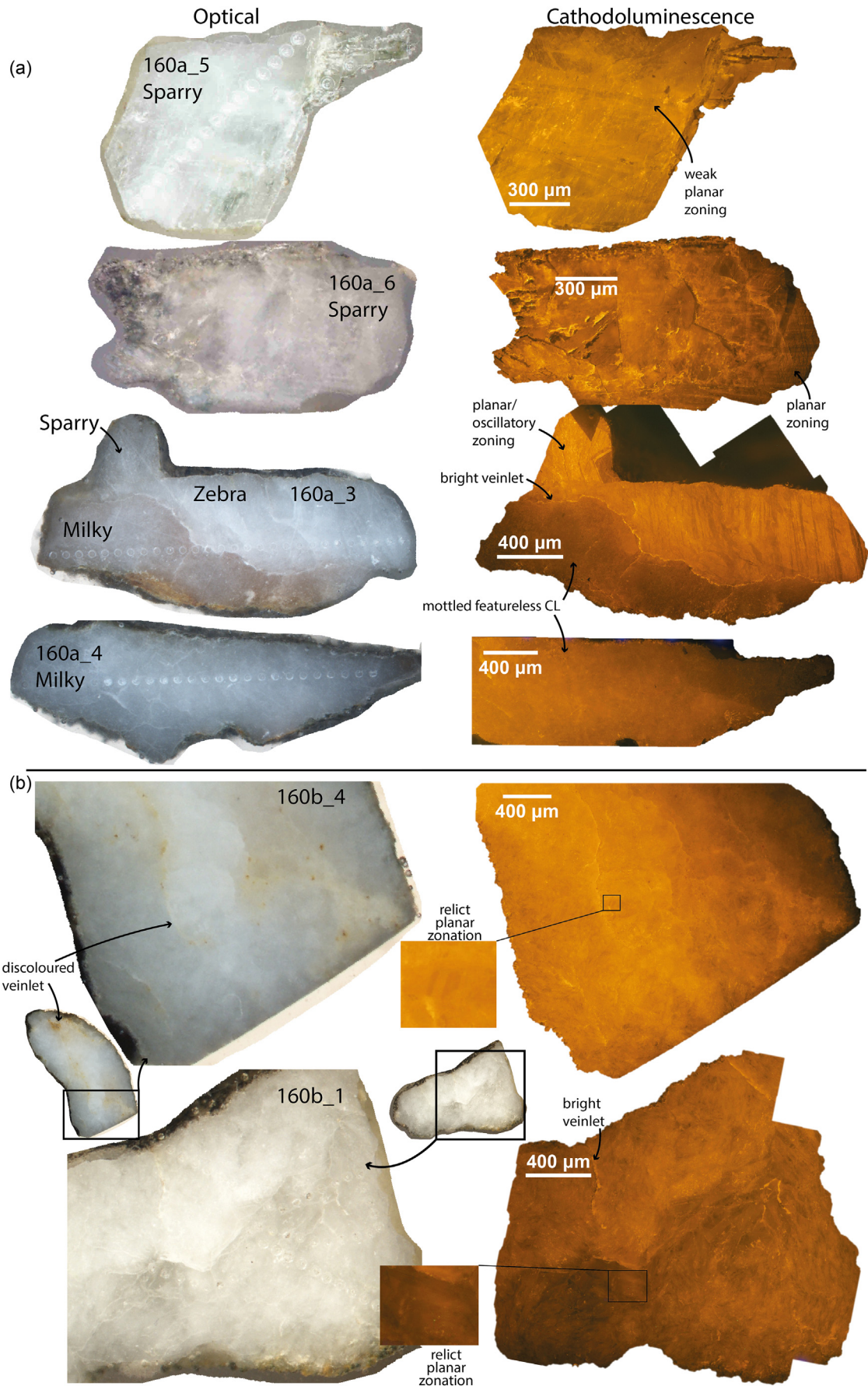


Fig. 3. Optical photographs and cathodoluminescence images of sample chips studied in detail. (a) Sample 160a, chips 3, 4, 5 and 6. (b) Sample 160b, chips 1 and 4.

planar, and can be correlated to the optical image. Enrichment and depletion in most elements are broadly correlative.

To compare the elemental composition of milky versus sparry calcite, four domains from two chips were examined for variation in their trace element signatures (Fig. 5a, c). The data are normalised to both the North American Shale Composite (NASC) and to a median value of this sample for easier comparison of enrichment and depletion. Based on texture alone, the sparry domains are interpreted as least altered, and the milky domain as the most altered. Overall, the NASC normalised plots show broadly consistent patterns between each of the domains, with some minor variation in the abundance of transition metals, large ion lithophile elements such as Sr and Ba, and heavy metals (Pb, Th, and U). Compared to the median values, the milky domain is depleted in V, Mn and Th, and is dominantly enriched in Pb. Other

elements are broadly similar to the median, or scatter about the median. The zebra-striped domain has some differences to the sparry calcite domains of this chip also, with notable depletion in V, Mn, Cu, Th and U. The sparry domains from chips 4 and 5 do not match, with varying enrichment and depletion. Regarding rare earth elements (REE), all samples show enrichment of middle REE over light REE, and either minor depletion of the HREE (Er to Lu) over the MREE (Dy, Ho), or flat HREE (milky domain). The plots indicate a minor negative Ce anomaly, and an enrichment in La over the other LREE. The size of the Ce anomaly, and absence of any notable Eu anomaly is consistent throughout each domain. The ratio Mn/Fe represents a ratio of CL emitter/inhibitor, and is thus commonly invoked as representing different fluid compositions. The Mn/Fe ratio for domains of 160a (Fig. 5c) shows that the difference between the sparry domains is the greatest, with the zebra-striped and

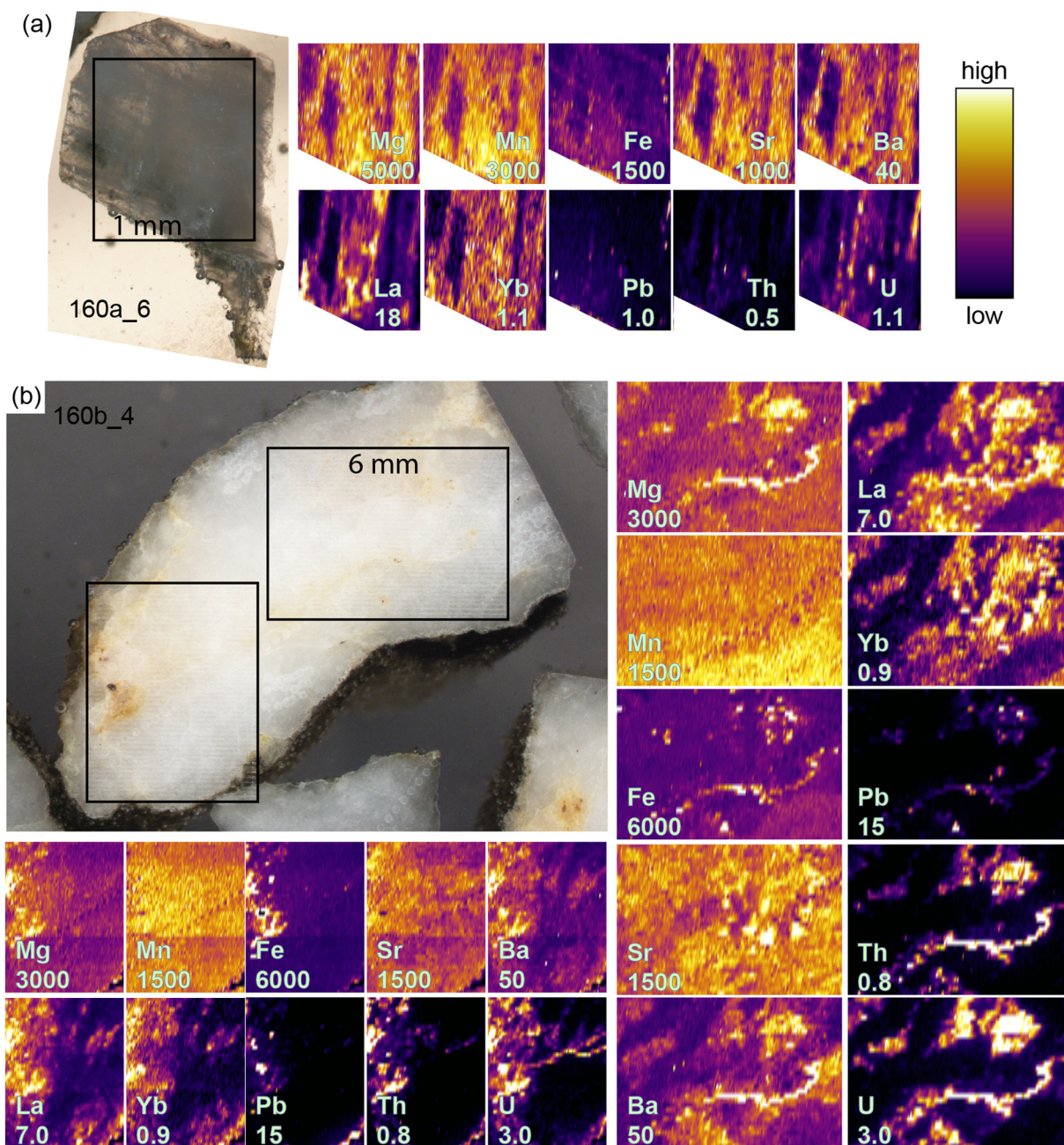


Fig. 4. Optical photographs and LA-ICP-MS trace element maps. Maximum concentration of the scale for each map is shown on the map as ppm ($\mu\text{g/g}$). (a) Sample 160a, chip 6. (b) Sample 160b, chip 4.

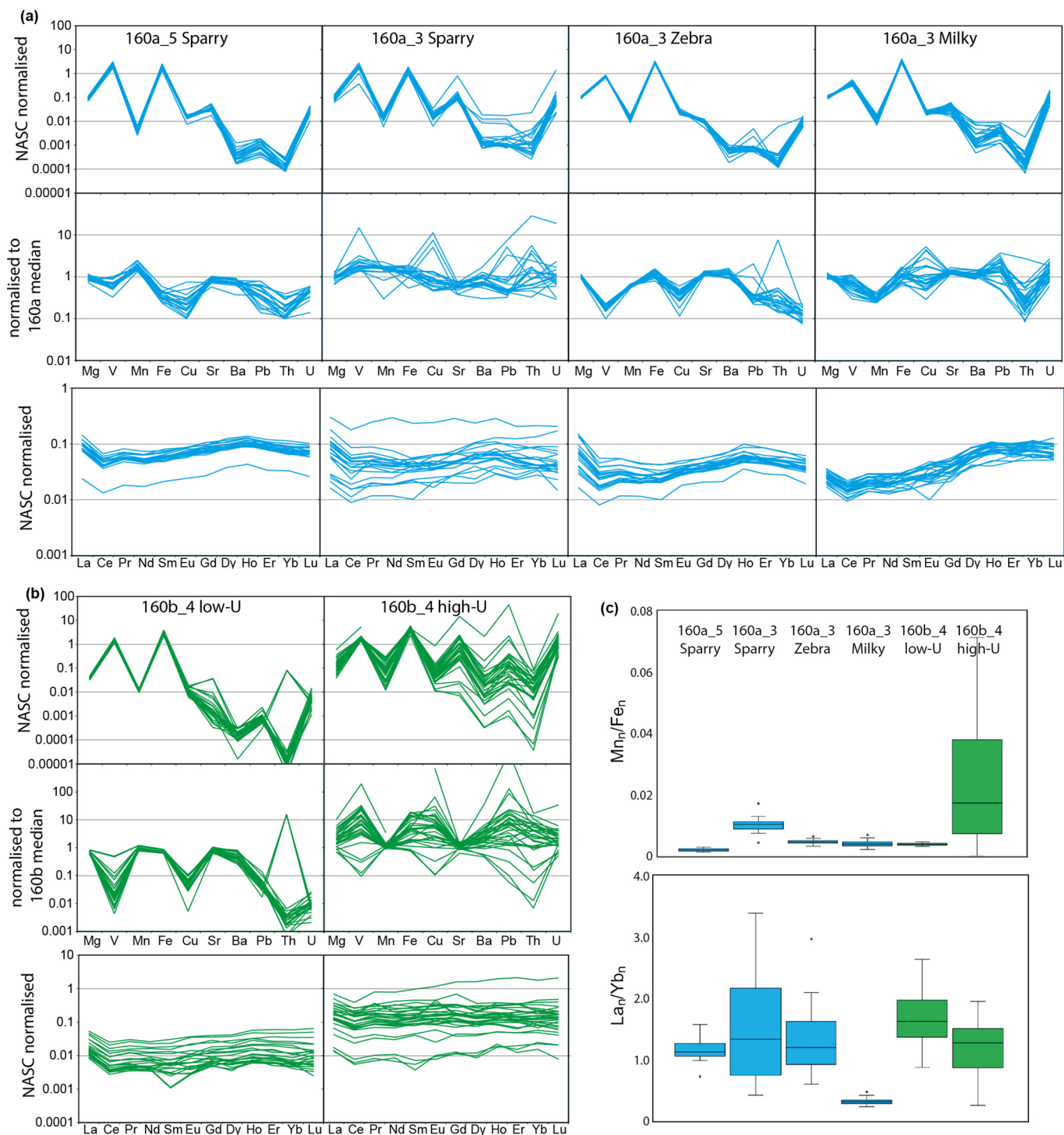


Fig. 5. LA-ICP-MS trace element data for different domains of calcite for each sample. Data are normalised to North American Shale Composite and to the median concentration based on all of the data from 160a. (a) Spider diagrams for sample 160a, chips 3 and 5. (b) Spider diagrams for sample 160b, chip 4. (c) Box plots comparing NASC-normalised Mn/Fe and La_T/Yb_N ratios for each sample domain.

milky domains similar to the sparry domain of chip 4. In contrast, the milky domain is distinctly different in REE signature (i.e. La/Yb) than the other domains.

5.2.2. Sample 160b

Trace element maps of two regions of chip 4 are shown in Fig. 4b. The maps show enrichment in all elements in domains that correlate with discoloured veinlets in the optical image. The variability of minor trace

elements across each map, such as the REE and Pb, Th and U, is much greater than that of elements with greater concentration (Mg, Mn, Fe and Sr).

Two domains from one chip were analysed (see Fig. 5b, c): the milky domain that is free from obvious veining (labelled as low-U), and the milky domain that comprises veinlets with obvious discolouration optically, and high uranium when viewed as an elemental map (labelled as high U). Both domains show broadly similar patterns to those of 160a, however, there are distinct differences between the domains that are

clear from the 160b median normalised plot. Whereas the milky domain is depleted in V, Cu, Pb, Th and U, the high-U domain is variably enriched in Mg, V, Fe, Cu, Ba, Pb, Th and U. The variation in the high-U is also greater than the other domains, but this likely reflects the spots being placed at varying distance to the most altered regions of the veinlet. The REE plots show flatter profiles than those of 160a, but with similar patterns of enrichment and similar-sized Ce anomalies. The Mn/Fe ratios shown as box plots (Fig. 5c) demonstrate a much greater Mn/Fe

ratio and variation in this ratio for the high-U domain, whereas the La/Yb of these domains are overlapping.

5.3. U-Pb geochronology

5.3.1. Sample 160a

A compilation of all U-Pb data comprising spot traverses across all seven chips is shown in Fig. 6a. The data reveal a fairly consistent

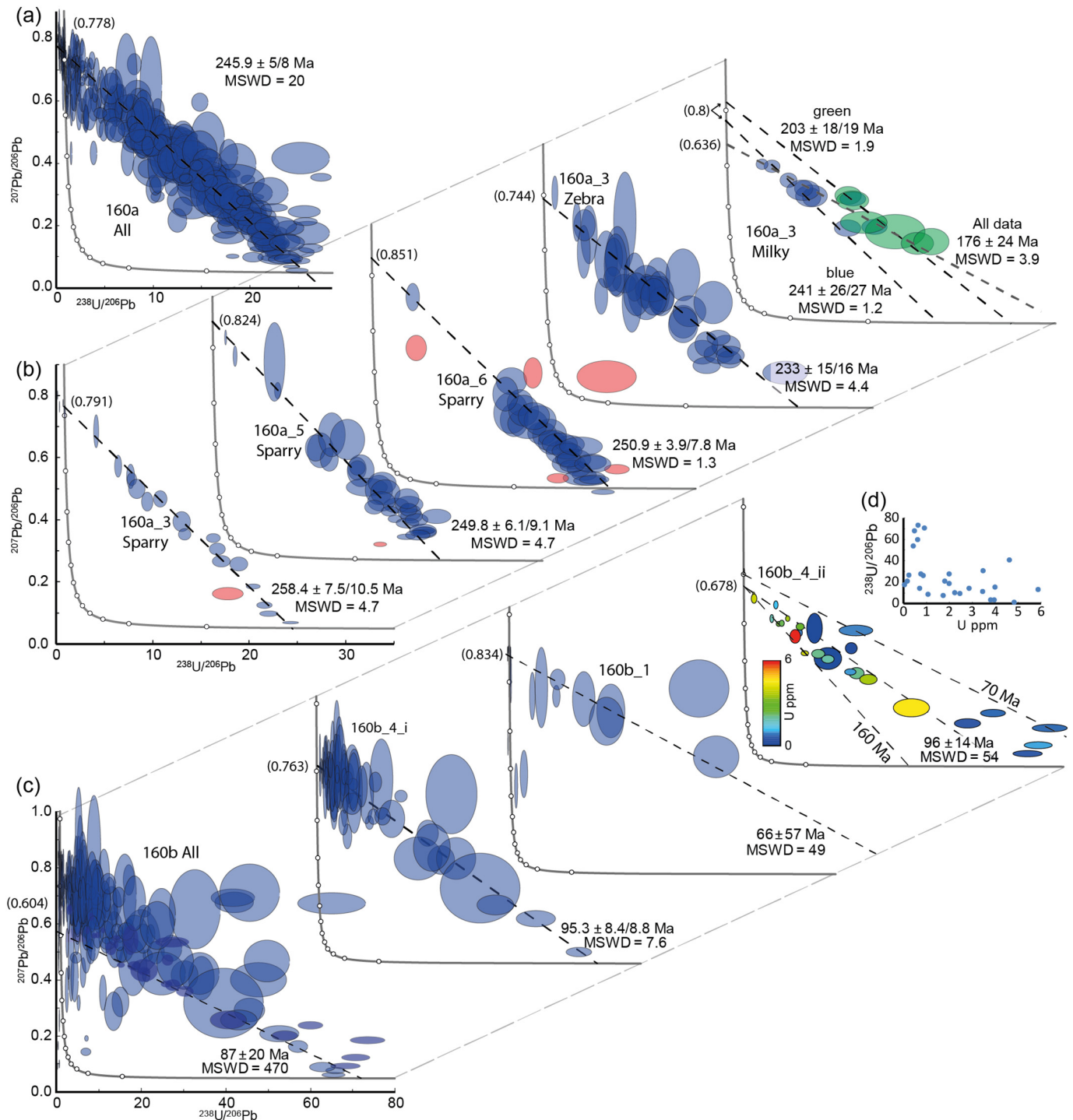


Fig. 6. Results of U-Pb geochronology plotted as Tera–Wasserburg diagrams (the scale for each plot remains the same), all uncertainties are plotted and quoted at 2σ . The age uncertainties are quoted as $\pm \alpha/\beta$, where α and β are without and with systematic uncertainty propagation, respectively (where these are the same at the level of quoted significant figures, only one uncertainty is quoted). (a) All dated domains of sample 160a. (b) Separate domains of sample 160a. (c) Plots from sample 160b. (d) U (ppm) versus $^{238}\text{U}/^{206}\text{Pb}$ ratio for the analysis of 160b_4_ii, where spots were located over a region of alteration. Red ellipses are outliers. Initial $^{207}\text{Pb}/^{206}\text{Pb}$ composition of each regression is provided in brackets.

population of data pointing to a lower intercept $^{206}\text{Pb}/^{238}\text{U}$ date of 245.9 ± 8 Ma. There are several outliers to this trend, and significant scatter at the high initial/low radiogenic lead of the array. Each textural domain of the four chips described above was dated individually. Sparry domains of chips 3, 5 and 6 reveal consistent lower intercept dates, with variable degrees of scatter (Fig. 6b). The small sparry pyramid on chip 3 yields a lower intercept date of 259.6 ± 10.5 Ma, with a MSWD of 5.4. Removing one distinct outlier improves this marginally to 258.4 ± 10.5 Ma, with a MSWD of 4.7. Sparry domains in chip 5 yields a lower intercept date of 258.7 ± 11.9 Ma (MSWD = 13). Removing a distinct outlier improves this considerably to 249.8 ± 9.1 Ma, with a MSWD of 4.7. The sparry chip 6 yields a lower intercept date of 246 ± 16 Ma, with a high MSWD of 17. There are clear outliers to the regression, suggesting some open-system behaviour or a younger domain. Removing these outliers shows that a single population can be obtained, with a lower intercept date of 250.9 ± 7.8 Ma (MSWD = 1.3).

The zebra-striped domain on chip 3 reveals a scattered array with a lower intercept date of 233 ± 16 Ma with a MSWD of 4.4. The milky domain yields a lower intercept date of 176 ± 24 Ma (MSWD = 3.9). This date which is much younger than the other domains, also exhibits a lower $^{207}\text{Pb}/^{206}\text{Pb}$ upper intercept composition (0.64 compared to >0.75). Because the initial Pb composition is anomalous in comparison to the rest of the sample, it is possible that this shallower regression results from a mixture of ages. To demonstrate that this data could result from a mixture of ages, we plot two regressions through an arbitrary grouping of the data using an estimated initial Pb composition of 0.75 ± 0.05 . These yield an older date of 241 ± 27 Ma (MSWD = 1.2), overlapping that demonstrated by the zebra-striped domain, and a younger date of 203 ± 19 Ma (MSWD = 1.9). We place no emphasis on these apparent dates in our interpretation that follows.

5.3.2. Sample 160b

The entire U-Pb dataset for this sample, comprising spots from all chips, is shown in Fig. 6c. The data reveal a scattered array of U-Pb data. The majority of the data have high initial to radiogenic lead compositions. A small amount of data have high radiogenic compositions, with a broad array to a lower intercept date around ca. 90 Ma. Data from chip 1 were mostly below detection limit, due to the very low Pb contents. A few scattered datapoints (Fig. 6c) yield a lower intercept date of 66 ± 57 Ma (MSWD = 49). Given the low abundance of data and anomalous outliers, this date is unreliable. Data from specific regions of chip 4 (Fig. 6c; 160b_4_i), i.e. those regions far from the discolouration, were also scattered, but much less so than the entire dataset. They yield a lower intercept date of 95.3 ± 8.8 Ma (MSWD = 7.6); although the data are scattered, the high degree of radiogenic lead provides some confidence to this date. A second dataset was generated from this sample (160b_4_ii), with spots placed across one of the discoloured veinlets cross-cutting the sample (see Fig. 3b). These spots provide a lower intercept date of 96 ± 14 Ma (MSWD = 54), which overlaps that derived from spots placed away from the veining. We have colour-coded the data according to their uranium content; although it would appear that the analyses with higher U/Pb ratios have lower U content, there is no clear trend between U/Pb ratio and U content (see Fig. 6d).

6. Discussion

6.1. Primary or secondary ages?

The original objective of this study was to determine the formation age of the calcite slickenfibres, and thus to determine the timing of fault slip along the Očkov fault. Although two samples have provided age constraints using U-Pb geochronology, this does not necessarily mean that these dates can be related to fault slip.

The sample 160a exhibits fairly consistent U-Pb age systematics across all of the dated chips, as demonstrated by Fig. 6. When dating

each domain separately, a clear pattern emerges: (1) a main date of ca. 250 Ma occurring in all chips, and (2) variably disturbed isotope systematics in some domains. Datapoints trending sub-horizontally at high $^{207}\text{Pb}/^{206}\text{Pb}$ compositions likely reflect U mobility (i.e. U addition). Conversely, some spots yield very low Pb-Pb and U-Pb ratios, perhaps reflecting U mobility in the form of U loss (see Roberts et al., 2020a). The sparry domains of three chips yield overlapping ages, and only minor disturbance. The zebra-striped domain has an overlapping age with the sparry domains, but with significant scatter around the regression. The milky domain exhibits elevated U/Pb ratios leading to apparently younger lower intercept ages; these isotope systematics may relate to younger growth, or to alteration. Since the milky domain likely represents recrystallization of a primary sparry texture, we interpret the latter interpretation that the data reflect disturbance of the U-Pb system. The age systematics are consistent with the sparry domains being the least altered, and the milky domain being the most altered. Simply based on its broadly correlative age, the zebra-striped domain may also be primary. Although not a feature of classical tiled slickenfibres growth (Passchier and Trouw 2005; Bons et al., 2012), this striping may reflect a form of antitaxial calcite growth that forms in *syn*-tectonic veins (see Bons et al., 2012).

The trace element data from sample 160a are not conclusive about the origin of any particular domain. The La/Yb ratio is distinctly different in the milky (altered) domain, but other signatures (e.g. Mn/Fe) are more variable between the sparry domains. The trace element map of chip 5 reveals enrichment/depletion in uranium that is correlative with other elements, including Mg and Mn; we interpret this as reflecting preservation of original primary zonation. Overall, we have no reason to suspect that the sparry domains, and the ca. 250 Ma they reveal, is not a primary feature. Thus, we suggest that this date reflects a period of slickenfibres growth bound by fault-slip displacements.

Sample 160b exhibits more complex isotope and elemental data than that of 160a. Analysis of differing regions across the chips exhibits highly scattered U-Pb data, with a lot of the data not falling on any definable regression (see Fig. 6c). Domains studied in detail in both chips yield apparent ages that are much younger than those of 160a, with chip 1 only giving a poorly defined regression that broadly overlaps the better defined regressions obtained from chip 4. The milky domain of chip 4 has considerable scatter particularly at the high common lead end of the regression. Based on several lines of evidence, we interpret 160b as recording recrystallisation of slickenfibres calcite, and mobilisation of the U and Pb isotopes: (1) the texture is variably milky, indicating microcrystalline calcite; (2) the CL texture is mottled with clear areas of veining, and sparse areas exhibiting relicts of planar or oscillatory zonation; (3) the U-Pb data are highly scattered, with low $^{207}\text{Pb}/^{206}\text{Pb}$ and low U/Pb ratios indicating potential loss of U compared to Pb, and high U/Pb domains (at similar $^{207}\text{Pb}/^{206}\text{Pb}$ values) reflecting gain of U relative to Pb; and (4) the trace element signatures and maps indicate that a large number of elements, including U and Pb, are enriched in the optically visible veining relative to the rest of the sample. This leaves the question, do the U-Pb data provide any constraints on the timing of this recrystallization? If a simple case for U mobility can be made, without Pb mobility, and the direction of mobility can be established (i.e. loss or gain of U), then there is potential that U-Pb data can provide minimum or maximum timing of the primary calcite formation. Based on comparison between high and low U domains in the trace element analysis (Fig. 5b), we interpret mobility of both U and Pb. This means that unpicking the isotope systematics are not straightforward. The persistence of Cretaceous lower intercept ages, could be taken as evidence that this represents the timing of recrystallisation. Conversely, the range of lower intercept dates from one localised region of spots of 160 Ma to 70 Ma (see Fig. 6c, 160b_4ii), suggests that this interpreted age should be treated with caution, and may only reflect an apparent age resulting from mobility of U and Pb. To further our understanding of when both fault slip and fluid-

driven recrystallisation occurred along this fault plane, we would need to observe more persistent isotope systematics across several samples.

6.2. Implications for regional tectonics

In the light of the above discussion, the ca. 250 Ma U–Pb age from the Očkov fault represents the first geochronological constraint on the timing of fault movement in the Prague syncline. The Očkov fault was assumed to connect with several other NE–SW-trending thrust faults along the southeastern limb of the Prague syncline (Fig. 1b) and together these faults were previously interpreted as having accommodated SE-directed ‘nappe tectonics’ during the Variscan orogeny in the Late Devonian (Melichar 2004). However, our fault-slip data and palaeostress estimations (see Supplementary Fig. S1) indicate that the fault belongs to a different set of faults, supported by the lack of evidence of a linkage of several thrust faults into a single system in this part of the Prague syncline (see Vacek and Žák, 2019 for discussion). The four different orientations of slickenfibres on the fault plane (Fig. 2b) further suggest that the movements along the Očkov fault were polyphase (see also Adamovič, 2002), and involved at least an early up-dip, top-to-the-S motion of the hangingwall (sample 160a; Fig. 2c) and later also two distinct dip-oblique movements (sample 160b; Fig. 2d). Our new U–Pb age yields a rather unexpected temporal constraint on these multiple slip episodes, indicating that reverse, dip-slip motion, which led to the earliest generation of slickenfibres (160a), was occurring at ca. 250 Ma.

During the earliest Triassic (at around 250 Ma), much of the Bohemian Massif presumably formed a basement block uplifted above the sea level (the Vindelician land), which sourced the surrounding marine basins (e.g. Ziegler, 1982). The former, already eroded Variscan orogen was in an overall extensional regime related to the earliest phases of the Pangaea break-up (e.g., Edel and Schneider, 1995; Arche and López-Gómez, 1996). However, in contrast to this overall extensional environment, Stille (1924) recognized an unconformity and compressional deformation at the Permian–Triassic boundary (the Pflanzian phase). Similarly, Szulc (2000) suggested a complex, temporally changing tectonic regime in Central Europe during Early to Middle Triassic, and compressional events were also reported from the southeastern margin of the Bohemian Massif (Franconian Line in Figs. 1 and 7a; e.g., Schröder, 1987; Hejl et al., 1997; Peterek et al., 1997; Schröder et al., 1997; Wagner et al., 1997; Vamvaka et al., 2014).

The Early Triassic intraplate compressional phase as inferred from the 250 Ma reverse slip along the Očkov fault also correlates with the apatite fission-track data of Glasmacher et al. (2002), who showed increased burial of the Prague Basin during the Early to Middle Triassic. Furthermore, the N–S compression calculated from our fault-slip data (Supplementary Fig. S1) is virtually identical in terms of orientation of the palaeostress axes and timing to that inferred for the Franconian Lineament truncating the southwestern margin of the Bohemian Massif (Phase 3 of Hejl et al., 1997 and Peterek et al., 1997). Taken together, these data suggest that the Vindelician land underwent compression at around 250 Ma. The possible geodynamic cause of this intra-plate compressional phase is difficult to establish and remains open to future research. Taking into account the palaeogeographic position of the Vindelician land, a plausible hypothesis may be short-lived compression in the overriding plate caused by the subduction of the southerly Palaeotethys Ocean (Fig. 7a).

Regarding sample 160b, there is considerable uncertainty over the accuracy of the calculated dates due to the interpreted mobility of U and Pb. Lower intercept ages ranging from 170 Ma to 60 Ma in an altered part of one chip, suggest that the primary age is likely to be much younger than the 250 Ma of sample 160a. The age of ca. 95 Ma exhibited from two separate regions, is our best estimate of the age of calcite recrystallisation. This age may represent: (1) calcite fibre growth during fault slip, with later fluid alteration leading to disturbance of the U and Pb isotopes; or (2) recrystallisation of an earlier formed calcite by alteration from fluids (which could also be related to fault slip). The sample 160b lies along

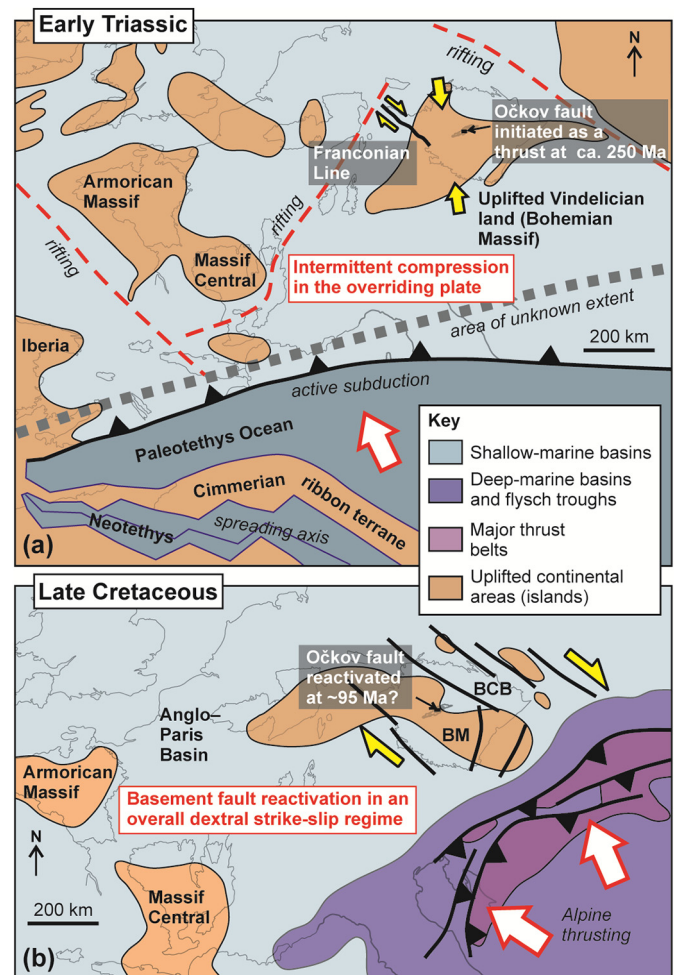


Fig. 7. Palaeogeographic reconstructions and principal tectonic elements of Central and Western Europe during (a) the Early to Middle Triassic and (b) the Late Cretaceous times (modified from Scheck-Wenderoth et al. 2008, and Uličný et al. 2009a, respectively). In both time periods, the Bohemian Massif underwent polyphase compressional deformation in response to far-field plate-boundary processes in the southerly to south-easterly Tethyan realm. Note that the reconstructions are plotted on a present-day map and thus cannot incorporate crustal deformations and rotations during the Mesozoic to Quaternary. See text for discussion. BCB – Bohemian Cretaceous Basin, BM – Bohemian Massif.

the same fault plane as 160a, thus it may be expected that fluid infiltration would affect all generations of slickenfibres; however the degree of U–Pb scatter and recrystallisation is variable across the samples. Could sample 160b be completely recrystallised and the isotopes mobilised without such disturbance of sample 160a? We tentatively speculate that 160b formed around ca. 95 Ma, at least in the age range of ca. 160 Ma to 70 Ma, and that fluid infiltration and isotope mobilisation occurred subsequently.

Although there is uncertainty regarding the accuracy of the apparent U–Pb date for 160b, the data indicate a likely Cretaceous timing of fluid infiltration with or without fault slip. The Cenomanian ca. 95 Ma date temporally overlaps with Africa/Eurasia plate convergence and with early stages of the Alpine orogeny (e.g., Kley and Voigt, 2008). The Vindelician landmass that persisted until the Jurassic (Ziegler, 1982) was replaced by several smaller islands that sourced the Bohemian Cretaceous Basin (Fig. 7b). At that time, the Lower successions of the Prague Basin were positioned at the margin of one of these islands (Fig. 7b). A ca. 95 Ma reactivation of the Očkov Fault is compatible with overall dextral shear along northerly NW–SE-trending major faults that controlled deposition in the Bohemian Cretaceous Basin and responded to thrusting in the Alps (Fig. 7b; Uličný, 2001; Uličný et al. 2009a, 2009b; Nádaskay et al., 2019).

In summary, the Očkov fault, previously considered as one of the 'classical' examples of Variscan orogenic thrusting in the Bohemian Massif, is in fact a structure resulting from polyphase post-orogenic intraplate deformation. The Variscan basement is cross-cut by ubiquitous brittle fractures, ranging from minor joints to large-scale faults, which have been frequently assumed as resulting from the Variscan orogeny. Following the example of the Očkov fault, it may be anticipated that future U-Pb dating of syntectonic calcite fibres may reveal previously unrecognized, multiple phases of post-Variscan intraplate deformation.

6.3. Implications for dating slickenfibres

U-Pb calcite geochronology is a growing method to determine the absolute timing of brittle deformation in the upper crust (see Roberts et al., 2020a). However, the details, caveats and best practise for this application are still being learnt. When in situ dating of zircon first took off in the 1990s with the growing number of ion microprobe instruments, it was quickly established that CL imaging should form a prerequisite for any isotope analyses. As Cornell and Austin Heggardt (2003) put it, there should be "no more blind dates with zircon". We claim that we are now standing at the same crossroads with carbonate geochronology, and for interpretations to be considered robust, U-Pb dates should be interpreted in the light of detailed sample petrography (such as CL imaging) and ideally elemental information (such as trace element mapping), and that dates without such information should be treated with caution. We also remind the community that although single dates can be interpreted as recording single events, if not well constrained they may possibly only reflect isotope mobility and an apparent age. Therefore, robust (low MSWD) overlapping ages from multiple samples are always desirable to establish the true age of events and processes.

Although data such as trace elements may help identify zones of alteration and primary calcite (Roberts et al., 2020a; Simpson et al., 2021), in this study we found no clear signatures in the trace element data that may be applicable to other study areas. It is likely that fluid resetting and fluid-driven recrystallisation will lead to elemental mobility that is strongly variable depending on local conditions.

7. Conclusions

We have used petrography, LA-ICP-MS trace element mapping, spot analyses and U-Pb geochronology, to analyse two examples of slickenfibres formed along the Očkov fault in the Prague Basin. Our results demonstrate that one sample has variably preserved primary textures, and yields a date of ca. 250 Ma, which we interpret as reflecting slickenfibre formation. The younger sample lacks preservation of primary texture, and is interpreted to have undergone variable degrees of recrystallisation. U and Pb have been mobilised in this sample, which limits our ability to interpret the ca. 95 Ma apparent age. Our dates indicate that the Očkov fault acted as a location of polyphase post-orogenic intraplate deformation, contrary to previous interpretations. Critically, we highlight that slickenfibre-based U-Pb dates do not unequivocally relate to fault motion, and may reflect fluid-flow post-slip with U and Pb mobilisation. As such, petrographic and compositional analyses are important requirements for interpreting calcite U-Pb data.

Declaration of competing interest

The authors declare that they have no known competing financial interests or personal relationships that could have appeared to influence the work reported in this paper.

Acknowledgements

Nick Roberts publishes with the permission of the Director of the British Geological Survey. This study was supported by the Czech Science Foundation through Grant No. 16-11500S (to Jiří Žák) and by the

Charles University through Centre for Geosphere Dynamics (UNCE/SCI/006) and project PROGRES Q45. We also acknowledge financial support from the Ministry of Culture of the Czech Republic through project DKRVO 2019–2023/1.IV.b (National Museum, 00023272). Robert Holder is thanked for providing the chip of Duff Brown calcite. We thank Stijn Glorie and an anonymous reviewer for their constructive comments, and Prof. Santosh for efficient editorial handling.

References

- Adamovič, J., 2002. Brittle Deformation of Devonian Limestones along the Očkov Fault, Čertovy Schody Quarry. Czech Geological Survey, Czech Republic, Geoscience Research Reports, pp. 12–13.
- Arche, A., López-Gómez, J., 1996. Origin of the Permian-Triassic Iberian Basin, Central-Eastern Spain. *Tectonophysics* 266, 443–464.
- Bajo, P., Hellstrom, J., Frisia, S., Drysdale, R., Black, J., Woodhead, J., Borsato, A., Zanchetta, G., Wallace, M.W., Regattieri, E., Haese, R., 2016. "Cryptic" diagenesis and its implications for speleothem geochronologies. *Quat. Sci. Rev.* 148, 17–28.
- Beaudoin, N., Lacombe, O., Roberts, N.M.W., Koehn, D., 2018. U-Pb dating of calcite veins reveals complex stress evolution and thrust sequence in the Bighorn Basin, Wyoming, USA. *Geology* 46, 1015–1018.
- Beaudoin, N.E., Labeur, A., Lacombe, O., Koehn, D., Billi, A., Hoareau, G., Boyce, A., John, C.M., Marchegiano, M., Roberts, N.M.W., Millar, I.L., 2020. Regional-scale paleofluid system across the Tuscan Nappe-Umbria-Marche Apennine Ridge (northern Apennines) as revealed by mesostructural and isotopic analyses of stylolite-vein networks. *Solid Earth* 11, 1617–1641.
- Bons, P.D., Elburg, M.A., Gomez-Rivas, E., 2012. A review of the formation of tectonic veins and their microstructures. *J. Struct. Geol.* 43, 33–62.
- Chlupáč, I., 1989. Geological Map 1:25,000, Sheet 12–413 Králův Dvůr. Prague, Czech Republic, Czech Geological Survey.
- Chlupáč, I., Havlíček, V., Kříž, J., Kůkal, Z., Štorch, P., 1998. Palaeozoic of the Barrandian (Cambrian to Devonian). Prague, Czech Republic, Czech Geological Survey, pp. 1–183.
- Coogan, L.A., Parrish, R.R., Roberts, N.M.W., 2016. Early hydrothermal carbon uptake by the upper oceanic crust: Insight from in situ U-Pb dating. *Geology* 44, 147–150.
- Cornell, D.H., Austin Heggardt, E., 2003. No more blind dates with zircon! EGS-AGU-EUG Joint Assembly, 2524, Nice, France.
- Coubal, M., Málek, J., Adamovič, J., Štěpančíková, P., 2015. Late Cretaceous and Cenozoic dynamics of the Bohemian Massif inferred from the paleostress history of the Lusitanian Fault Belt. *J. Geodyn.* 87, 26–49.
- Danišík, M., Migoň, P., Kuhlemann, J., Evans, N.J., Dunkl, I., Frisch, W., 2010. Thermochronological constraints on the long-term erosional history of the Karakoram Mts., Central Europe. *Geomorphology* 117, 78–89.
- Danišík, M., Štěpančíková, P., Evans, N.J., 2012. Constraining long-term denudation and faulting history in intraplate regions by multisystem thermochronology: an example of the Sudetic Marginal Fault (Bohemian Massif, central Europe). *Tectonics* 31, TC2003. <https://doi.org/10.1029/2011TC003012>.
- DeWolf, C.P., Halliday, A.N., 1991. U-Pb dating of a remagnetized Paleozoic limestone. *Geophys. Res. Lett.* 18, 1445–1448.
- Edel, J.B., Schneider, J.L., 1995. The Late Carboniferous to Early Triassic geodynamic evolution of Variscan Europe in the light of magnetic overprints in Early Permian rhyolites from the northern Vosges (France) and central Black Forest (Germany). *Geophys. J. Int.* 122, 858–876.
- Filip, J., Suchý, V., 2004. Thermal and tectonic history of the Barrandian Lower Paleozoic, Czech Republic: is there a fission-track evidence for Carboniferous–Permian overburden and pre-Westphalian alpinotype thrusting? *B. Geosci.* 79, 107–112.
- Glasmacher, U.A., Mann, U., Wagner, G.A., 2002. Thermotectonic evolution of the Barrandian, Czech Republic, as revealed by apatite fission-track analysis. *Tectonophysics* 359, 381–402.
- Goodfellow, B.W., Viola, G., Bingen, B., Nuriel, P., Kylander-Clark, A.R., 2017. Palaeocene faulting in SE Sweden from U-Pb dating of slickenfibre calcite. *Terra Nova* 29, 321–328.
- Hajná, J., Žák, J., Kachlík, V., Chadima, M., 2012. Deciphering the Variscan tectonometric overprint and deformation partitioning in the Cadomian basement of the Teplá-Barrandian unit, Bohemian Massif. *Int. J. Earth Sci.* 101, 1855–1873.
- Halavínová, M., Melichar, R., Slobodník, M., 2008. Hydrothermal veins linked with the Variscan structure of the Prague Synform (Barrandien, Czech Republic): resolving fluid-wall rock interaction. *Geol. Q.* 52, 309–320.
- Hansman, R.J., Albert, R., Gerdes, A., Ring, U., 2018. Absolute ages of multiple generations of brittle structures by U-Pb dating of calcite. *Geology* 46, 207–210.
- Havlíček, V., 1963. Tectogenetic disruption of the Barrandian Paleozoic. *J. Geol. Sci. Geol.* 1, 77–102.
- Havlíček, V., 1981. Development of a linear sedimentary depression exemplified by the Prague Basin (Ordovician–Middle Devonian; Barrandian area – central Bohemia). *Sbor. Geol. Věd. Geol.* 35, 7–48.
- Hejl, E., Coyle, D., Lal, N., Van den Haute, P., Wagner, P.A., 1997. Fission-track dating of the western border of the Bohemian massif: thermochronology and tectonic implications. *Geol. Rundsch.* 86, 210–219.
- Hill, C.A., Polyak, V.J., Asmerom, Y., Provencio, P., 2016. Constraints on a Late Cretaceous uplift, denudation, and incision of the Grand Canyon region, southwestern Colorado Plateau, USA, from U-Pb dating of lacustrine limestone. *Tectonics* 35, 896–906.
- Hoareau, G., Crognier, N., Lacroix, B., Aubourg, C., Roberts, N.M.W., Niemi, N., Branellec, M., Beaudoin, N., Ruiz, I.S., 2021. Combination of $\Delta 47$ and U-Pb dating in tectonic calcite veins unravel the last pulses related to the Pyrenean Shortening (Spain). *Earth Planet. Sci. Lett.* 553, 116636.

- Holdsworth, R.E., McCaffrey, K.J.W., Dempsey, E., Roberts, N.M.W., Hardman, K., Morton, A., Feely, M., Hunt, J., Conway, A., Robertson, A., 2019. Natural fracture propping and earthquake-induced oil migration in fractured basement reservoirs. *Geology* 47, 700–704.
- Jochum, K.P., Weis, U., Stoll, B., Kuzmin, D., Yang, Q., Raczek, I., Jacob, D.E., Stracke, A., Birbaum, K., Frick, D.A., Günther, D., 2011. Determination of reference values for NIST SRM 610–617 glasses following ISO guidelines. *Geostand. Geoanal. Res.* 35, 397–429.
- Kley, J., Voigt, T., 2008. Late Cretaceous intraplate thrusting in Central Europe: effect of Africa–Iberia–Europe convergence, not Alpine collision. *Geology* 36, 839–842.
- Li, Q., Parrish, R.R., Horstwood, M.S.A., McArthur, J.M., 2014. U–Pb dating of cements in Mesozoic ammonites. *Chem. Geol.* 376, 76–83.
- Machel, H.G., 1985. Cathodoluminescence in calcite and dolomite and its chemical interpretation. *Geosci. Can.* 12, 161–168.
- Machel, H.G., 2000. Application of cathodoluminescence to carbonate diagenesis. In: Pagel, M., Barbin, V., Blanc, P., Ohnenstetter, D. (Eds.), *Cathodoluminescence in Geosciences*. Springer, Berlin, Germany, pp. 271–301.
- Malkovský, M., 1987. The Mesozoic and Tertiary basins of the Bohemian Massif and their evolution. *Tectonophysics* 137, 31–42.
- Martínez Catalán, J.R., 2012. The Central Iberian arc, an orocline centered in the Iberian Massif and some implications for the Variscan belt. *Int. J. Earth Sci.* 101, 1299–1314.
- Melichar, R., 2004. Tectonics of the Prague Synform: a hundred years of scientific discussion. *Krystalinikum* 30, 167–187.
- Miranda, T.S., Neves, S.P., Celestino, M.A.L., Roberts, N.M., 2020. Structural evolution of the Cruzeiro do Nordeste shear zone (NE Brazil): Brasiliano–Pan–African–ductile-to-brittle transition and Cretaceous brittle reactivation. *J. Struct. Geol.* 141, 104203. <https://doi.org/10.1016/j.jsg.2020.104203>.
- Mottram, C.M., Kellett, D.A., Barresi, T., Zwingmann, H., Friend, M., Todd, A., Percival, J.B., 2020. Syncing fault rock clocks: Direct comparison of U–Pb carbonate and K–Ar illite fault dating methods. *Geology* 48, 1179–1183.
- Nádaskay, R., Žák, J., Sláma, J., Sidorinová, T., Valečka, J., 2019. Deciphering the Late Paleozoic to Mesozoic tectonosedimentary evolution of the northern Bohemian Massif from detrital zircon geochronology and heavy mineral provenance. *Int. J. Earth Sci.* 108, 2653–2681.
- Nance, R.D., Gutiérrez-Alonso, G., Keppie, J.D., Linnemann, U., Murphy, J.B., Quesada, C., Strachan, R.A., Woodcock, N.H., 2010. Evolution of the Rheic Ocean. *Gondwana Res.* 17, 194–222.
- Nuriel, P., Weinberger, R., Kylander-Clark, A.R.C., Hacker, B.R., Craddock, J.P., 2017. The onset of the Dead Sea transform based on calcite age-strain analyses. *Geology* 45, 587–590.
- Nuriel, P., Craddock, J., Kylander-Clark, A.R., Uysal, I.T., Karabacak, V., Dirik, R.K., Hacker, B.R., Weinberger, R., 2019. Reactivation history of the North Anatolian fault zone based on calcite age-strain analyses. *Geology* 47, 465–469.
- Opluštil, S., Cleal, C.J., 2007. A comparative analysis of some late Carboniferous basins of Variscan Europe. *Geol. Mag.* 144, 417–448.
- Opluštil, S., Schmitz, M.D., Cleal, C.J., Martinek, K., 2016. A review of the Middle–Late Pennsylvanian west European regional substages and floral biozones, and their correlation to the Geological Time Scale based on new U–Pb ages. *Earth-Sci. Rev.* 154, 301–335.
- Oren, O., Nuriel, P., Kylander-Clark, A.R., Haviv, I., 2020. Evolution and propagation of an active plate boundary: U–Pb ages of fault-related calcite from the Dead Sea Transform. *Tectonics* 39. <https://doi.org/10.1029/2019TC005888> e2019TC005888.
- Parrish, R.R., Parrish, C.M., Lasalle, S., 2018. Vein calcite dating reveals Pyrenean orogen as cause of Paleogene deformation in southern England. *J. Geol. Soc. Lond.* 175, 425–442.
- Passchier, C.W., Trouw, R.A., 2005. *Microtectonics*. Springer Science & Business Media, Berlin.
- Paton, C., Hellstrom, J., Paul, B., Woodhead, J., Hergt, J., 2011. *lollite*: freeware for the visualisation and processing of mass spectrometric data. *J. Anal. Atom Spectrom.* 26, 2508–2518.
- Peterek, A., Rauche, H., Schröder, B., Franzke, H.J., Bankwitz, P., Bankwitz, E., 1997. The late- and post-Variscan tectonic evolution of the Western Border fault zone of the Bohemian massif (WBZ). *Geol. Rundsch.* 86, 191–202.
- Ring, U., Gerdes, A., 2016. Kinematics of the Alpenrhein–Bodensee graben system in the Central Alps: Oligocene/Miocene transtension due to formation of the Western Alps arc. *Tectonics* 35, 1367–1391.
- Roberts, N.M.W., Walker, R.J., 2016. U–Pb geochronology of calcite-mineralized faults: absolute timing of rift-related fault events on the Northeast Atlantic margin. *Geology* 44, 531–534.
- Roberts, N.M.W., Rasbury, E.T., Parrish, R.R., Smith, C.J., Horstwood, M.S., Condon, D.J., 2017. A calcite reference material for LA-ICP-MS U–Pb geochronology. *Geochem. Geophys. Geosyst.* 18, 2807–2814.
- Roberts, N.M.W., Drost, K., Horstwood, M.S., Condon, D.J., Chew, D., Drake, H., Milodowski, A.E., McLean, N.M., Smye, A.J., Walker, R.J., Haslam, R., 2020a. Laser ablation inductively coupled plasma mass spectrometry (LA-ICP-MS) U–Pb carbonate geochronology: strategies, progress, and limitations. *Geochronology* 2, 33–61.
- Roberts, N.M.W., Lee, J.K., Holdsworth, R.E., Jeans, C., Farrant, A.R., Haslam, R., 2020b. Near-surface Palaeocene fluid flow, mineralisation and faulting at Flamborough Head, UK: new field observations and U–Pb calcite dating constraints. *Solid Earth* 11, 1931–1945.
- Röhlich, P., 2007. Structure of the Prague basin: the deformation diversity and its causes (Czech Republic). *B Geosci.* 82, 175–182.
- Scheck-Wenderoth, M., Krzywicki, P., Zühlke, R., Maystrenko, Y., Froitzheim, N., McCann, T., 2008. Permian to Cretaceous tectonics. *The Geology of Central Europe Volume 2: Mesozoic and Cenozoic*. Geol Soc Spec Pub, pp. 999–1030.
- Scholz, D., Tolzmann, J., Hoffmann, D.L., Jochum, K.P., Spötl, C., Riechmann, D.F.C., 2014. Diagenesis of speleothems and its effect on the accuracy of $^{230}\text{Th}/\text{U}$ -ages. *Chem. Geol.* 387, 74–86.
- Schröder, B., 1987. Inversion tectonics along the western margin of the Bohemian Massif. *Tectonophysics* 137, 93–100.
- Schröder, B., Ahrendt, H., Peterek, A., Wemmer, K., 1997. Post-Variscan sedimentary record of the SW margin of the Bohemian massif: a review. *Geol. Rundsch.* 86, 178–184.
- Schulmann, K., Konopásek, J., Janoušek, V., Lexa, O., Lardeaux, J.M., Edel, J.B., Štípská, P., Ulirch, S., 2009. An Andean type Palaeozoic convergence in the Bohemian Massif. *Compt. Rendus Geosci.* 341, 266–286.
- Schulmann, K., Lexa, O., Janoušek, V., Lardeaux, J.M., Edel, J.B., 2014. Anatomy of a diffuse cryptic suture zone: an example from the Bohemian Massif, European Variscides. *Geology* 42, 275–278.
- Simpson, A., Glorie, S., Morley, C.K., Roberts, N.M.W., Gillespie, J., Lee, J.K., 2021. In-situ calcite U–Pb geochronology of hydrothermal veins in Thailand: new constraints on Indosinian and Cenozoic deformation. *J. Asian Earth Sci.* 206, 104649. <https://doi.org/10.1016/j.jseas.2020.104649>.
- Slobodník, M., Melichar, R., Hurai, V., Bakker, R.J., 2012. Litho-stratigraphic effect on Variscan fluid flow within the Prague synform, Barrandian: evidence based on C, O, Sr isotopes and fluid inclusions. *Mar. Pet. Geol.* 35, 128–138.
- Smeraglia, L., Aldega, L., Billi, A., Carminati, E., Di Fiore, F., Gerdes, A., Albert, R., Rossetti, F., Vignaroli, G., 2019. Development of an intrawedge tectonic mélange by out-of-sequence thrusting, buttressing, and intraformational rheological contrast, Mt. Massico Ridge, Apennines, Italy. *Tectonics* 38, 1223–1249.
- Smith, P.E., Farquhar, R.M., Hancock, R.G., 1991. Direct radiometric age determination of carbonate diagenesis using U–Pb in secondary calcite. *Earth Planet. Sci. Lett.* 105, 474–491.
- Stille, H., 1924. *Grundfragen der vergleichenden Tektonik*. Borntraeger, Berlin, p. 443.
- Suchý, V., Rozkošný, I., Žák, K., Franc, J., 1996. Epigenetic dolomitization of the Přídolí formation (Upper Silurian), the Barrandian basin, Czech Republic: implications for burial history of lower Paleozoic strata. *Int. J. Earth Sci.* 85, 264–277.
- Suchý, V., Dobeš, P., Filip, J., Stejskal, M., Zeman, A., 2002. Conditions for veining in the Barrandian Basin (lower Palaeozoic), Czech Republic: evidence from fluid inclusion and apatite fission track analysis. *Tectonophysics* 348, 25–50.
- Szulc, J., 2000. Middle Triassic evolution of the northern peri-Tethys area as influenced by early opening of the Tethys Ocean. *Ann. Soc. Geol. Pol.* 70, 1–48.
- Uličný, D., 2001. Depositional systems and sequence stratigraphy of coarse-grained deltas in a shallow-marine, strike-slip setting: the Bohemian Cretaceous Basin, Czech Republic. *Sedimentology* 48, 599–628.
- Uličný, D., Laurin, J., Čech, S., 2009a. Controls on clastic sequence geometries in a shallow-marine, transtensional basin: the Bohemian Cretaceous Basin, Czech Republic. *Sedimentology* 56, 1077–1114.
- Uličný, D., Špičáková, L., Grygar, R., Svobodová, M., Čech, S., Laurin, J., 2009b. Palaeodrainage systems at the basal unconformity of the Bohemian Cretaceous Basin: roles of inherited fault systems and basement lithology during the onset of basin filling. *B Geosci.* 84, 577–610.
- Vacek, F., Žák, J., 2019. A lifetime of the Variscan orogenic plateau from uplift to collapse as recorded by the Prague Basin, Bohemian Massif. *Geol. Mag.* 156, 485–509.
- Vamvaka, A., Siebel, W., Chen, F., Rohrmüller, J., 2014. Apatite fission-track dating and low-temperature history of the Bavarian Forest (southern Bohemian Massif). *Int. J. Earth Sci.* 103, 103–119.
- Ventura, D., Lisker, F., 2003. Long-term landscape evolution of the northeastern margin of the Bohemian Massif: apatite fission-track data from the Erzgebirge (Germany). *Int. J. Earth Sci.* 92, 691–700.
- Wagner, G.A., Coyle, D.A., Duyster, J., Henjes-Kunst, F., Peterek, A., Schröder, B., Stöckhert, B., Wemmer, K., Zulauf, G., Ahrendt, H., Bischoff, R., Hejl, E., Jacobs, J., Menzel, D., Lal, N., Van den Haute, P., Vercoutere, C., Welzel, B., 1997. Post-Variscan thermal and tectonic evolution of the KTB site and its surroundings. *J. Geophys. Res.* 102, 18221–18232.
- Weinberger, R., Nuriel, P., Kylander-Clark, A.R., Craddock, J.P., 2020. Temporal and spatial relations between large-scale fault systems: evidence from the Sinai–Negev shear zone and the Dead Sea Fault. *Earth-Sci. Rev.* 211, 103377. <https://doi.org/10.1016/j.earscirev.2020.103377>.
- Williams, R.T., Goodwin, L.B., Sharp, W.D., Mozley, P.S., 2017. Reading a 400,000-year record of earthquake frequency for an intraplate fault. *P Natl. Acad. Sci.* 114, 4893–4898.
- Williams, R.T., Mozley, P.S., Sharp, W.D., Goodwin, L.B., 2019. U–Th dating of syntectonic calcite veins reveals the dynamic nature of fracture cementation and healing in faults. *Geophys. Res. Lett.* 46, 12900–12908.
- Winchester, J.A., 2002. Palaeozoic amalgamation of Central Europe: new results from recent geological and geophysical investigations. *Tectonophysics* 360, 5–21.
- Žák, J., Kraft, P., Hajná, J., 2013. Timing, styles, and kinematics of Cambro–Ordovician extension in the Teplá–Barrandian Unit, Bohemian Massif, and its bearing on the opening of the Rheic Ocean. *Int. J. Earth Sci.* 102, 415–433.
- Ziegler, P.A., 1982. Triassic rifts and facies patterns in Western and Central Europe. *Geol. Rundsch.* 71, 747–772.
- Zulauf, G., 2001. Structural style, deformational mechanisms and paleodifferential stress along an exposed crustal section: constraints on the rheology of quartzofeldspathic rocks at supra- and infrastructural levels (Bohemian Massif). *Tectonophysics* 332, 211–237.